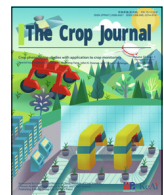


Contents lists available at ScienceDirect

The Crop Journal

journal homepage: www.keaipublishing.com/en/journals/the-crop-journal/

Panicle-3D: A low-cost 3D-modeling method for rice panicles based on deep learning, shape from silhouette, and supervoxel clustering



Dan Wu^{a,1}, Lejun Yu^{a,b,1}, Junli Ye^c, Ruifang Zhai^c, Lingfeng Duan^c, Lingbo Liu^a, Nai Wu^c, Zedong Geng^c, Jingbo Fu^c, Chenglong Huang^c, Shangbin Chen^a, Qian Liu^{a,b,*}, Wanneng Yang^{c,*}

^a Britton Chance Center for Biomedical Photonics, Wuhan National Laboratory for Optoelectronics, and Key Laboratory of Ministry of Education for Biomedical Photonics, Department of Biomedical Engineering, Huazhong University of Science and Technology, Wuhan 430074, Hubei, China

^b School of Biomedical Engineering, Hainan University, Haikou 570228, Hainan, China

^c National Key Laboratory of Crop Genetic Improvement, National Center of Plant Gene Research, Huazhong Agricultural University, Wuhan 430070, Hubei, China

ARTICLE INFO

Article history:

Received 10 August 2021

Revised 23 October 2021

Accepted 21 March 2022

Available online 25 March 2022

Keywords:

Panicle phenotyping
Deep convolutional neural network
3D reconstruction
Shape from silhouette
Point-cloud segmentation
Ray tracing
Supervoxel clustering

ABSTRACT

Self-occlusions are common in rice canopy images and strongly influence the calculation accuracies of panicle traits. Such interference can be largely eliminated if panicles are phenotyped at the 3D level. Research on 3D panicle phenotyping has been limited. Given that existing 3D modeling techniques do not focus on specified parts of a target object, an efficient method for panicle modeling of large numbers of rice plants is lacking. This paper presents an automatic and nondestructive method for 3D panicle modeling. The proposed method integrates shoot rice reconstruction with shape from silhouette, 2D panicle segmentation with a deep convolutional neural network, and 3D panicle segmentation with ray tracing and supervoxel clustering. A multiview imaging system was built to acquire image sequences of rice canopies with an efficiency of approximately 4 min per rice plant. The execution time of panicle modeling per rice plant using 90 images was approximately 26 min. The outputs of the algorithm for a single rice plant are a shoot rice model, surface shoot rice model, panicle model, and surface panicle model, all represented by a list of spatial coordinates. The efficiency and performance were evaluated and compared with the classical structure-from-motion algorithm. The results demonstrated that the proposed method is well qualified to recover the 3D shapes of rice panicles from multiview images and is readily adaptable to rice plants of diverse accessions and growth stages. The proposed algorithm is superior to the structure-from-motion method in terms of texture preservation and computational efficiency. The sample images and implementation of the algorithm are available online. This automatic, cost-efficient, and nondestructive method of 3D panicle modeling may be applied to high-throughput 3D phenotyping of large rice populations.

© 2022 2022 Crop Science Society of China and Institute of Crop Science, CAAS. Production and hosting by Elsevier B.V. on behalf of KeAi Communications Co., Ltd. This is an open access article under the CC BY-NC-ND license (<http://creativecommons.org/licenses/by-nc-nd/4.0/>).

1. Introduction

Rice (*Oryza sativa*) is one of the most important food crops in the world, which feeds over half of the global population [1,2]. Geneticists and breeders have made great efforts to identify rice accessions with ideal characteristics for crop growth and production [3–5]. The rice panicle, whose characteristics influence grain yield, is the target of many rice phenotyping studies [6–8].

Image-based techniques have become increasingly important in crop phenotyping. These techniques, generally adopting one or more imaging methods such as visible, hyperspectral, thermal infrared, and tomographic imaging, have greatly advanced the progress of high-throughput phenotyping and have potential to replace conventional phenotyping methods, which depend mainly on low-efficiency manual manipulation [9,10]. Deep learning methods have shown impressive performance in many areas and have increasing application in phenotyping research, especially for detection and counting tasks. Pound et al. [11] presented a deep-learning approach with a new dataset for localizing and counting wheat spikes and spikelets. Lu et al. [12] solved the in-field counting problem of maize tassels with a local count regression network. Xiong et al. [13] proposed a robust method for field

* Corresponding authors.

E-mail addresses: qliu@hainanu.edu.cn (Q. Liu), ywn@mail.hzau.edu.cn (W. Yang).

¹ These authors contributed equally to this work.

rice panicle segmentation by simple linear iterative clustering and convolutional neural-network classification. With the combination of image processing techniques, panicle traits can be efficiently quantified from images. In the method proposed by Duan et al. [14], the panicle numbers of rice plants were determined using multiangle imaging and artificial neural network segmentation. Wu et al. [15] developed an image analysis-based method to quantify the grain numbers of detached panicles. But nondestructive image-based panicle phenotyping accuracy is greatly reduced by self-occlusions that commonly appear in rice canopy images. Such interference can be largely eliminated if panicles are phenotyped at the three-dimensional (3D) level. However, relatively few studies have considered acquiring panicle traits from 3D rice models, given that an efficient method for modeling large numbers of rice plants is lacking.

Generally, a more comprehensive understanding of plant features can be obtained from 3D plant models than from single-view or multiple-view plant images, and analysis of links between canopy architecture characteristics and photosynthetic capacity can be performed based on 3D plant models [16]. The generation of a 3D plant model is an essential step for subsequent trait extraction and can be achieved using various techniques, including laser scanning, structured light (SL), time of flight (TOF), and structure from motion (SFM) [17]. The laser-scanning technique is used mostly in the case of miniplots or experimental fields. This approach can obtain 3D point clouds of high resolution and accuracy [17]. Usually, canopy-associated parameters, including plant height, leaf inclination angle, and plant area density, can be extracted automatically or by manual interpretation [18,19]. The structured-light technique is also superior in resolution and accuracy, though the long time required for imaging limits its application to high-throughput phenotyping. Nguyen et al. [20] established a structured light-based 3D reconstruction system to phenotype plant heights, leaf numbers, leaf sizes and internode distances of cabbages, cucumbers, and tomatoes. Time-of-flight imaging, despite its low resolution, was successfully applied to corn [21,22], and phenotypic parameters of the corn plant, including leaf length, leaf width, leaf area, stem diameter, stem height and leaf angle, could be estimated. This technique was also used to measure cotton plant height under field conditions [23]. SFM reconstruction, in contrast to active illumination-based laser scanning, SL and TOF, is a passive approach that represents the current state-of-the-art technique in multiview stereo vision. Pound et al. [24] presented an automatic SFM-based approach to recover 3D shapes of rice plants in which the outputs were surface-mesh structures consisting of a series of small planar sections. This method was then employed by Burgess et al. [25] to investigate the potential effects of wind-induced perturbation of the plant canopy on light patterning, interception, and photosynthetic productivity. It was combined with ray tracing [26] to characterize the light environment within an intercrop. The reconstruction software packages VisualSfM [27] and PMVS [28], on which Pound et al.'s method [24] was based, accept as input a set of images with no special shooting mode required, and have shown high robustness in various cases. They have also been applied to 3D phenotyping of other crops including corn [29], strawberry [30], and grapevine [31]. Another multiview stereo algorithm for 3D modeling is space carving [32]. This method reconstructs the 3D shape according to the photoconsistency of calibrated images around the scene of interest. Simpler than space carving is the shape-from-silhouette (SFS) algorithm, which requires foreground segmentation for each input image. Both space carving and SFS are good at reconstructing high curvature and thin structures [33]. Another novel method is modeling by hyperspectral imaging, which was investigated by Liang et al. [34] and Behmann et al. [35].

Despite the many approaches available for 3D plant modeling, a reconstruction system for rice panicles is lacking. In general, a 3D panicle model for rice can be developed by two methods: cutting off panicles from rice plants and reconstructing 3D panicle models with images of excised panicles, or developing a 3D shoot rice model and then segmenting panicles from the rest of the plant. Examples of the first method are PI-Plat [36] and X-ray-based work [37]. Given that panicles were cut from stems, neither estimation of the panicle spatial distributions nor dynamic observations were possible. In addition, the phenotyping process was slowed by manual collection of panicles. For the second method, a 3D shoot rice model can be generated, while there are no algorithms for automatic 3D panicle segmentation. Panicle segmentation of a 3D shoot rice model is more complex than 2D panicle segmentation of rice canopy images. It is difficult to distinguish panicles from the remaining parts of a 3D shoot rice model using color information or geometric features. Although there are some well-built neural networks for 3D classification and segmentation, such as VoxNet [38] and PointNet [39], the input data sizes are quite limited (an occupancy grid of $32 \times 32 \times 32$ for VoxNet and thousands of points for PointNet). Current computing power cannot deal with a shoot rice model that may contain hundreds of thousands of points. No such current technology focuses on nondestructive 3D panicle modeling.

In this paper, we present an automatic and nondestructive 3D modeling method for rice panicles. The SFS algorithm is used to generate the shoot rice model, and then a deep convolutional neural network and supervoxel clustering are used to perform 3D panicle segmentation. Totally 50 rice plants of various genotypes and growth stages were used to test the proposed algorithm and comparisons with the SFM method were performed. The results show that the proposed method is well qualified to recover the 3D shapes of rice panicles from multiview images and is easily adaptable to rice plants of diverse accessions and growth stages. It is superior to the SFM method in terms of texture preservation and computational efficiency.

2. Materials and methods

2.1. Multiview imaging system

An indoor 3D imaging system named Panicle-3D was developed to acquire multiview rice images. The imaging system (Fig. 1A) comprised mainly a digital single-lens reflex camera (EOS 760D, Canon, Tokyo, Japan), a turntable (MERA200, Red Star Yang Technology, Wuhan, Hubei, China), a group of LED lights (Philips, Amsterdam, Netherlands), a PLC control unit (CP1H, OMRON, Kyoto, Japan) and a computer (Gigabyte Technology, New Taipei City, Taiwan, China). The camera was kept at a fixed position, and the focal length was fixed to 18 mm throughout image acquisition. A rice plant was placed on the turntable rotating at a constant speed of 2° per second, and the camera automatically shot at two-second intervals during the revolution. The acquisition time of each image was recorded with millisecond precision for calibration. It took approximately 4 min to phenotype a single rice plant, including manual handling and image acquisition.

2.2. Rice materials

Fifty rice plants of various genotypes and growth stages were tested with the Panicle-3D system. These plants, including 25 rice accessions selected from 529 *O. sativa* accessions [40] and 25 mutants of ZH11, were grown in plastic pots. Images of the 25 accessions from 529 *O. sativa* accessions were taken between the flowering and dough grain stages. Images of the 25 ZH11 mutants

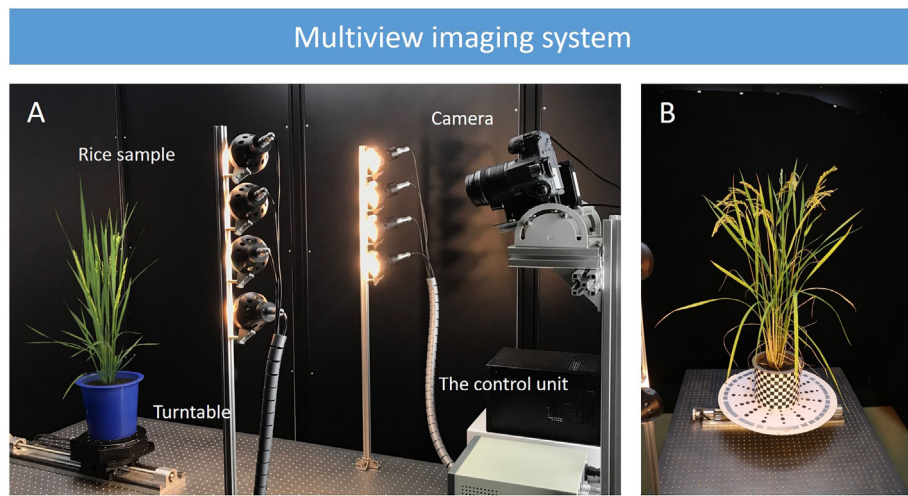


Fig. 1. Multiview imaging system. (A) The multiview imaging system. (B) A rice canopy image in side view.

were taken between the dough-grain and mature-grain stages. For each rice plant, 90 side-view images, as shown in Fig. 1B, were acquired. A total of 4500 images were collected to form a dataset for 3D panicle modeling.

2.3. The concepts of four 3D models

We introduce the four 3D models for later reference. The shoot rice model (SRM) refers to the stuffed point cloud of a rice canopy. The shoot rice model reconstructed by the SFS algorithm does not contain color information. The surface shoot rice model (SSRM) refers to the surface point cloud of a rice canopy. The panicle model (PM) refers to the stuffed point cloud of all panicles in a rice canopy. The panicle model acquired by 3D segmentation of the shoot rice model reconstructed by the SFS algorithm does not contain color information. The surface panicle model (SPM) refers to the surface point cloud of all panicles in a rice canopy. Both the surface shoot rice model and the surface panicle model contain color information obtained by identifying correspondences between image pixels and spatial points.

2.4. The pipeline of the 3D panicle modeling algorithm

The flow diagram of the proposed 3D panicle modeling algorithm is shown in Fig. 2. It includes 2D panicle segmentation, 3D shoot rice reconstruction, and 3D panicle segmentation. The shoot rice model, surface shoot rice model, panicle model, and surface panicle model were generated from multiview rice canopy images. Following are the detailed steps of the algorithm, taking one rice plant as an example. (1) The SegNet-Panicle model for 2D panicle segmentation: 60 field rice images [13] of 1971×1815 and 4000×4500 pixel resolution (Fig. 2A) and the corresponding label images (Fig. 2B) were used to generate 2370 rice images of 360×480 resolution (Fig. 2C) and the corresponding label images (Fig. 2D). These images were used to train SegNet [41] to obtain a SegNet-Panicle model (Fig. 2E) for 2D panicle segmentation. (2) Multiview rice canopy images: for a single rice plant, 90 images of 6000×4000 resolution (Fig. 2F) were taken automatically from different views in the imaging chamber. All these images were calibrated with a rotation-axis calibration technique following Zhang [42]. (3) Rice canopy silhouette images: all original rice canopy images (Fig. 2F) were segmented using fixed-color thresholding to obtain a canopy silhouette images (Fig. 2G) in which each pixel is categorized into either a rice or background pixel. (4) Panicle-

segmented images: all original rice canopy images (Fig. 2F) were segmented using the pretrained SegNet-Panicle model to obtain panicle-segmented images (Fig. 2H) in which each pixel was assigned as either a panicle or background pixel. (5) Shoot rice model and surface shoot rice model: the shoot rice model (Fig. 2I) was reconstructed by the SFS algorithm using 90 canopy silhouette images, and then the surface shoot rice model (Fig. 2J) was obtained by rendering the surface points of the shoot rice model. (6) Panicle model and surface panicle model: the panicle model (Fig. 2K) was obtained by performing 3D panicle segmentation of the shoot rice model, and then the surface panicle model (Fig. 2L) was obtained as the intersection of the panicle model and the surface shoot rice model.

2.5. Camera calibration

The SFS algorithm requires calibration parameters corresponding to rice image sequences. To obtain these parameters, the rotation axis was set as the Z axis of the world coordinate system. Because the object underwent pure rotation, the origin of the world coordinate system could be an arbitrary point on the rotation axis. A simple technique was developed to determine the orientation of the rotation axis relative to the camera. First, a chessboard pattern with 15×10 white and black squares and 14×9 inner corners (see in Supplementary files) was printed and attached to a Perspex panel. A few images of the chessboard panel in different orientations were taken with the camera from close distances. These close-up shots were used to calculate the intrinsic camera parameters by Zhang's calibration method [42]. The chessboard panel was then placed on the top surface of the turntable to acquire an image sequence over 360° of rotation for extrinsic parameter calibration. The pixel image coordinates of each inner corner of the chessboard pattern were tracked automatically with OpenCV [43]. Given the intrinsic camera parameters, the extrinsic parameters including the rotation parameters and the translation parameters that related the world coordinate system to the camera coordinate system were calculated from the correspondences of spatial coordinates and pixel coordinates of the chessboard corners. A different assignment of the world coordinate system determines a different group of spatial coordinates of the corners, which further leads to a different group of rotation and translation vectors. Note that the translation vectors corresponding to the extrinsic calibration images theoretically have the same value when the rotation axis is taken as the Z-axis of the world

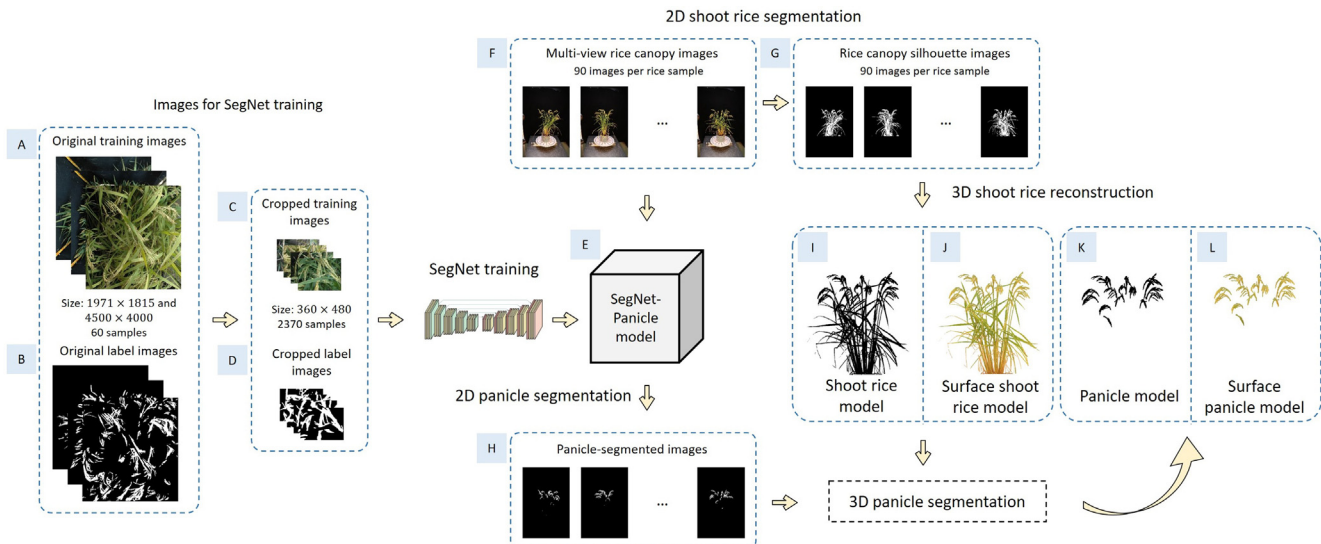


Fig. 2. The pipeline of the 3D panicle modeling algorithm. (A) Original training images. (B) Original label images. (C) Cropped training images. (D) Cropped label images. (E) The SegNet-Panicle model for 2D panicle segmentation. (F) Multiview rice canopy images. (G) Rice canopy silhouette images. (H) Panicle-segmented images. (I) The shoot rice model reconstructed by the SFS algorithm. (J) The surface shoot rice model generated by texture extrusion. (K) The panicle model generated by performing 3D panicle segmentation on the shoot rice model. (L) The surface panicle model generated by taking the intersection of the surface shoot rice model and the panicle model.

coordinate system. Any other assignment of the Z-axis leads to variation between the translation vectors. Accordingly, the extrinsic parameters that corresponded to the extrinsic calibration images with the adopted assignment were determined by finding the group of translation vectors with minimum variance. The rotation vectors that corresponded to the extrinsic calibration images determined a regression plane from which an initial rotation vector could be selected. The selection of the initial rotation vector could be arbitrary because only relative positions would be considered in SFS reconstruction. Once the initial rotation vector and the translation vector were determined, the extrinsic parameters corresponding to the rice image sequences were calculated according to the acquisition time and rotation speed.

2.6. 2D panicle segmentation

The aim of 2D panicle segmentation was to acquire panicle-segmented images that provide essential information for 3D panicle segmentation. In a panicle-segmented image, each pixel is categorized as either a panicle pixel or a nonpanicle pixel. Considering that the panicle colors are similar to those of other parts of rice plants and that panicles appear in various shapes and poses, it is difficult to segment panicles by color thresholding or conventional machine-learning algorithms that depend on hand-engineered features. Instead, a well-built deep convolutional neural network (CNN), SegNet [41], was employed to perform robust 2D panicle segmentations. The SegNet architecture is composed of an encoder network, a corresponding decoder network, and a pixelwise classification layer. It takes as input an image of 360×480 resolution and generates a prediction image of the same size. The network should be trained with an adequate number of training samples before it can be applied for panicle segmentation. The use of SegNet is similar to that of general deep learning methods, and the detailed implementation steps are described as follows.

(1) Training set: Sixty rice images (including 50 images of 1971×1815 resolution and 10 images of 4500×4000 resolution) with corresponding ground-truth labels were selected from the Panicle-Seg dataset [13]. These rice images were acquired in complex field environments, involving

diverse challenges for panicle segmentation, such as variations in rice accession, illumination imbalance, and cluttered background caused by soil and water reflection. Because the size of these images did not match the input image size of SegNet, each image and ground-truth was first extended to a larger size by adding a black background and then cut into small patches of 360×480 resolution. Each image of 1971×1815 resolution was extended to 2160×1920 resolution and cut into 24 patches. Each image of 4500×4000 resolution was extended to 4680×4320 resolution and cut into 117 patches. In total, 2370 patches of 360×480 resolution were acquired, and all these patches were used as the training set.

- (2) Training SegNet: The network was trained using stochastic gradient descent [44] with a fixed learning rate of 0.001 and momentum of 0.9. The model was accepted after 100 epochs through the training set when the training loss converged and no increases in accuracy were observed. This model was named the SegNet-Panicle model.
- (3) Segmentation with the SegNet-Panicle model: All 4500 rice canopy images of 6000×4000 resolution for 3D panicle modeling were segmented using the pretrained SegNet-Panicle model. To meet the input image size of SegNet, each rice image was extended to 6120×4320 resolution by adding a black background and then cut into 153 patches of 360×480 resolution. Each patch was segmented with the pretrained SegNet-Panicle model. The segmentation results of 153 patches were spliced into a single result image of 6120×4320 resolution. The extended black area was removed and the image was trimmed to obtain a final image of 6000×4000 resolution.

2.7. 3D reconstruction of rice shoot

The SFS algorithm, also known as visual hull construction, was employed to generate the shoot rice model. The algorithm recovers an object shape by carving away empty regions using a silhouette sequence [45]. The general processes for a rice shoot are as follows: (1) acquire the calibration parameters corresponding to 90 rice canopy images by the method described in section 2.5; (2) acquire

90 canopy silhouette images using fixed color thresholding; and (3) initialize a volume that is large enough to contain a rice shoot and carve away the regions of the volume that once projected out of the canopy silhouettes.

The silhouette images for shoot rice reconstruction were the binary segmentation results of the rice canopy. For rice images taken in the Panicle-3D imaging system in which the color of the scene background was unlikely to appear in rice canopies and the pixel values of the background were significantly lower than that of the rice shoot, the silhouettes were extracted automatically with fixed color thresholding according to the discriminants given below:

$$\begin{cases} g/b \geq 1 \\ r/b \geq 1 \\ b+g+r > m \end{cases} \quad (1)$$

where r , g and b represent respectively the gray values of the red, green, and blue channels of pixels in the original rice canopy images. The silhouette was the combination of all the pixels that satisfied these inequalities. It should be mentioned that the exposure and brightness were higher in the images of the 25 accessions selected from 529 *O. sativa* accessions than in the images of the 25 ZH11 mutants. The threshold value m was set 80 for 2250 shoot rice images of 25 ZH11 mutants and to 150 for 2250 shoot rice images of 25 of 529 *O. sativa* accessions.

After the silhouette sequence and corresponding calibration parameters were obtained, the shoot rice model was computed volumetrically. This was done by initializing 1,048,576,000 ($1024 \times 1024 \times 1000$) cubic voxels of $1 \times 1 \times 1 \text{ mm}^3$ that represented a cuboid volume of $1024 \times 1024 \times 1000 \text{ mm}^3$, then projecting each voxel to the silhouette sequence and carving away all the voxels that had once projected outside the silhouettes.

Besides the SFS reconstruction, the surface points of the shoot rice model were also rendered by extruding the original RGB rice images along viewing rays. Texture extrusion was implemented by the ray-tracing technique. For each pixel that belonged to the rice shoot silhouette, a ray was cast from the viewpoint across the pixel into space and the intersection of the viewing ray and the shoot rice model was calculated. Actually, the viewing ray was a list of occupancy intervals during intersection calculations.

The voxel corresponding to the pixel was the voxel of intersection nearest to the viewpoint. The intersection voxel was drawn with an average of colors as seen from the RGB rice image sequence. The textured surface shoot rice model was obtained by assembling all colored voxels.

2.8. 3D panicle segmentation

Apparently, panicle segmentation at the three-dimensional level is more difficult than for 2D images. The problem does not lie merely in the similarities of the panicle voxel colors to those of other parts of the rice plant. Some progressive deep learning techniques targeted on 3D objects were also influenced because of the shortage of 3D training datasets and because of memory intensiveness. We accordingly developed a solution for 3D panicle segmentation that innovatively integrated 2D pixelwise panicle segmentation with ray tracing and supervoxel clustering.

The detailed procedures of 3D panicle segmentation are illustrated in Fig. 3. First, presegmentation was performed to acquire mask points (Fig. 3B). This operation required 2D panicle-segmented images, as previously mentioned. The presegmentation resembled the rendering of the shoot rice model in the application of a ray-tracing technique. For each pixel that belonged to the canopy silhouette, its corresponding voxel on the shoot rice model was determined by intersection calculation. The shoot rice model voxels were scored by introducing a parameter, referred to as the score, that indicated the probability of the voxel's belonging to the panicle. Each voxel achieved an initial score of zero. The score increased when the voxel was seen to be foreground in the panicle-segmented images and decreased when the voxel was seen to be background. After scoring was complete, mask points (Fig. 3B) were obtained by removing voxels whose score was zero or negative. For better observation, a partial view of the mask points is presented in Fig. 3C. Paralleling the presegmentation was the generation of supervoxels by voxel-cloud connectivity segmentation (VCCS) [46]. The VCCS algorithm works directly in the 3D space using voxel relationships to produce oversegmentations. It constructs an adjacency graph for the voxel cloud by searching the voxel K-dimensional tree, then selects seed points to initialize the supervoxels, and finally iteratively assigns voxels to

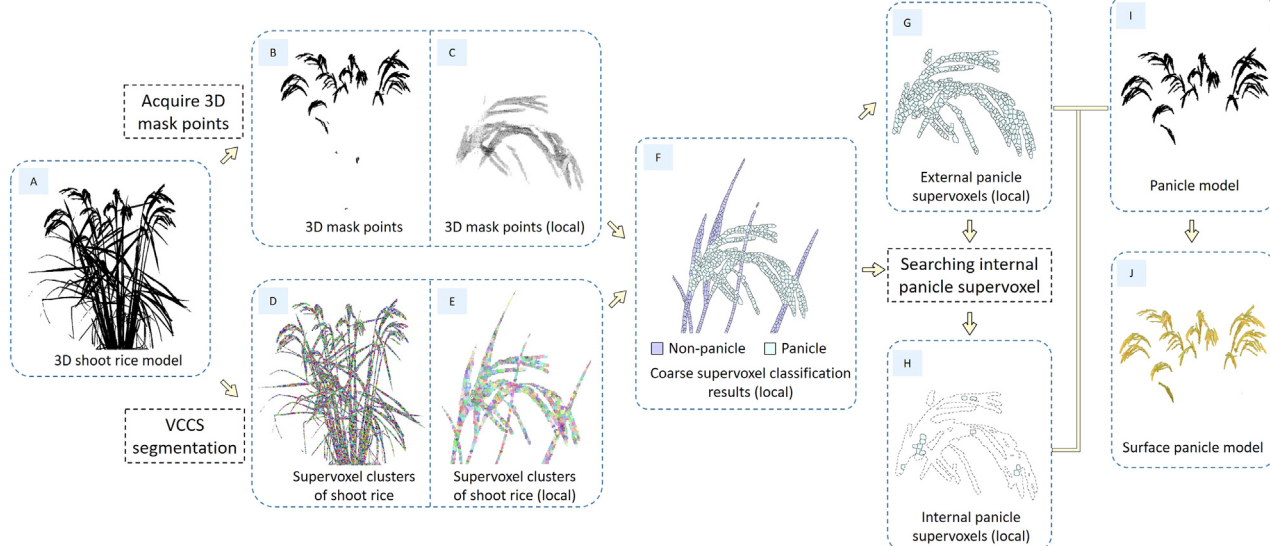


Fig. 3. The pipeline of 3D panicle segmentation. (A) 3D shoot rice model. (B) 3D mask points generated by presegmentation according to panicle-segmented images. (C) 3D mask points (local view). (D) Supervoxel clusters of shoot rice generated by VCCS segmentation. (E) Supervoxel clusters of shoot rice (local view). (F) Coarse supervoxel classification results (local view). (G) External panicle supervoxels (local view). (H) Internal panicle supervoxels (local view). (I) The panicle model. (J) The surface panicle model.



Fig. 4. The results of 2D panicle segmentation using the SegNet-Panicle model. The original rice images are shown in the first column, the manual segmentation results using Photoshop software are shown in the second column, and the results using the SegNet-Panicle model are shown in the last column. (A), (B), and (C) are three mutants of ZH11.

supervoxels using flow constrained clustering. Generally, three parameters, λ , μ and ϵ , which control the influence of color, spatial distance and geometric similarity, respectively, need to be specified when the VCCS algorithm is run. We expected that supervoxels would occupy a relatively spherical space, which would be more desirable for further processing. Accordingly, the values of λ and ϵ were set to zero, which meant that only spatial distance was considered. A sample result of VCCS and a partial view are shown in Fig. 3D and E, respectively. After the shoot rice model was transformed into a set of supervoxels, coarse supervoxel segmentation was performed to classify each supervoxel into either panicle supervoxel or nonpanicle supervoxel. If a supervoxel contained one or more mask points, it was classified as a panicle supervoxel; otherwise, it was classified as a nonpanicle supervoxel. The result of coarse supervoxel segmentation is shown in Fig. 3F. It is easy to see that only external panicle supervoxels (Fig. 3G) can be recognized, given that the mask points were a set of surface points,

there being no opportunity for an internal panicle supervoxel to contain a mask point. Accordingly, a simple criterion was adopted to detect the internal panicle supervoxels (Fig. 3H) that were not recognized by coarse supervoxel segmentation. If a supervoxel was adjacent to identified panicle supervoxels in three or more directions, it was also classified as a panicle supervoxel. The ultimate panicle model (Fig. 3I) was the combination of all identified external and internal panicle supervoxels. Derived from the shoot rice model, the panicle model did not contain color information. A textured surface panicle model was also created (Fig. 3J) from the intersection of the panicle model and the surface shoot rice model.

2.9. Performance evaluation

To evaluate the performance of the SegNet-Panicle model, 25 images that originated from 25 ZH11 mutants for 3D panicle



Fig. 5. The results of 3D shoot rice reconstruction and 3D panicle segmentation. The original rice images and the corresponding 2D panicle segmentation results are shown in the first and third columns, respectively. The surface shoot rice models are shown in the second column. The surface panicle models from the side view and top view are shown in the fourth and last columns, respectively. (A, B) Rice samples from 529 *O. sativa* accessions at the flowering stage. (C, D) Mutants of ZH11 at the mature stage.

modeling were selected to build the test set. For each mutant, the first image of the multiview image sequence was selected. The ground-truth labels of the 25 test images were obtained by manual segmentation using Photoshop software [47]. Automatic segmentation of the test images was performed with the SegNet-Panicle model. Four indicators: precision, recall, IoU, and F-measure of the test images, were calculated for evaluation of 2D panicle segmentation accuracy.

We also investigated how the number of panicle-segmented images that were used would affect the efficiency and accuracy of 3D panicle segmentation on the shoot rice model using 25 ZH11 mutants. When the algorithm was tested on each plant, all 90 images taken from different angles were used to generate the shoot rice model and the surface shoot rice model. The panicle-segmented images were obtained using the pretrained SegNet-Panicle model. Then, different numbers of panicle-segmented images, in turn from 3 to 90, were used to segment panicle points from the shoot rice model. Manual segmentations on shoot rice models were conducted using CloudCompare [48] software for comparison with automatic segmentation. The IoU was adopted to evaluate the performance of 3D panicle segmentation. The calculation formula of IoU at the three-dimensional level is given below:

$$\text{IoU} = \frac{\text{TP}}{\text{TP} + \text{FP} + \text{FN}}$$

where TP refers to points that were categorized as panicle points both by the algorithm and by manual segmentation. FP refers to points that were categorized as panicle points by the algorithm but were manually classified as nonpanicle points. FN refers to points that were manually classified as panicle points but were not recognized by the algorithm. The ranges of IoU were from 0 to 1, and a higher value of IoU indicated better 3D panicle segmentation.

VisualSfM software (retrieved at <https://ccwu.me/vsfm/>), which represents the current state-of-the-art technology of multiview stereo reconstruction, was tested on the dataset for comparison with the proposed method. To make use of VisualSfM, the background in each original image was colored black and the rice pixels remained unchanged, since these images were acquired in a static camera capture system, while VisualSfM was adaptable to moving camera systems. For a single rice plant, 90 background-removed images were used to generate the surface shoot rice model. Then, noise points on the surface shoot rice model were filtered out using color thresholding. Finally, manual segmentation of the surface shoot rice model was per-

formed using CloudCompare software to obtain the surface panicle model.

2.10. Requirements for data processing

Computations were performed on Ubuntu 18.04 64-bit and Windows 10 64-bit dual operating systems with an NVIDIA

GeForce RTX 2080Ti GPU configured. The training of SegNet and 2D panicle segmentation were performed on the Ubuntu system. All other processes were performed on the Windows system. The project for 3D shoot rice reconstruction and 3D panicle segmentation was developed in the C++ language combined with OpenCV and PCL libraries [49]. OpenMP [50] and CUDA [51] were adopted to speed up the calculations. The source codes of the algorithm and

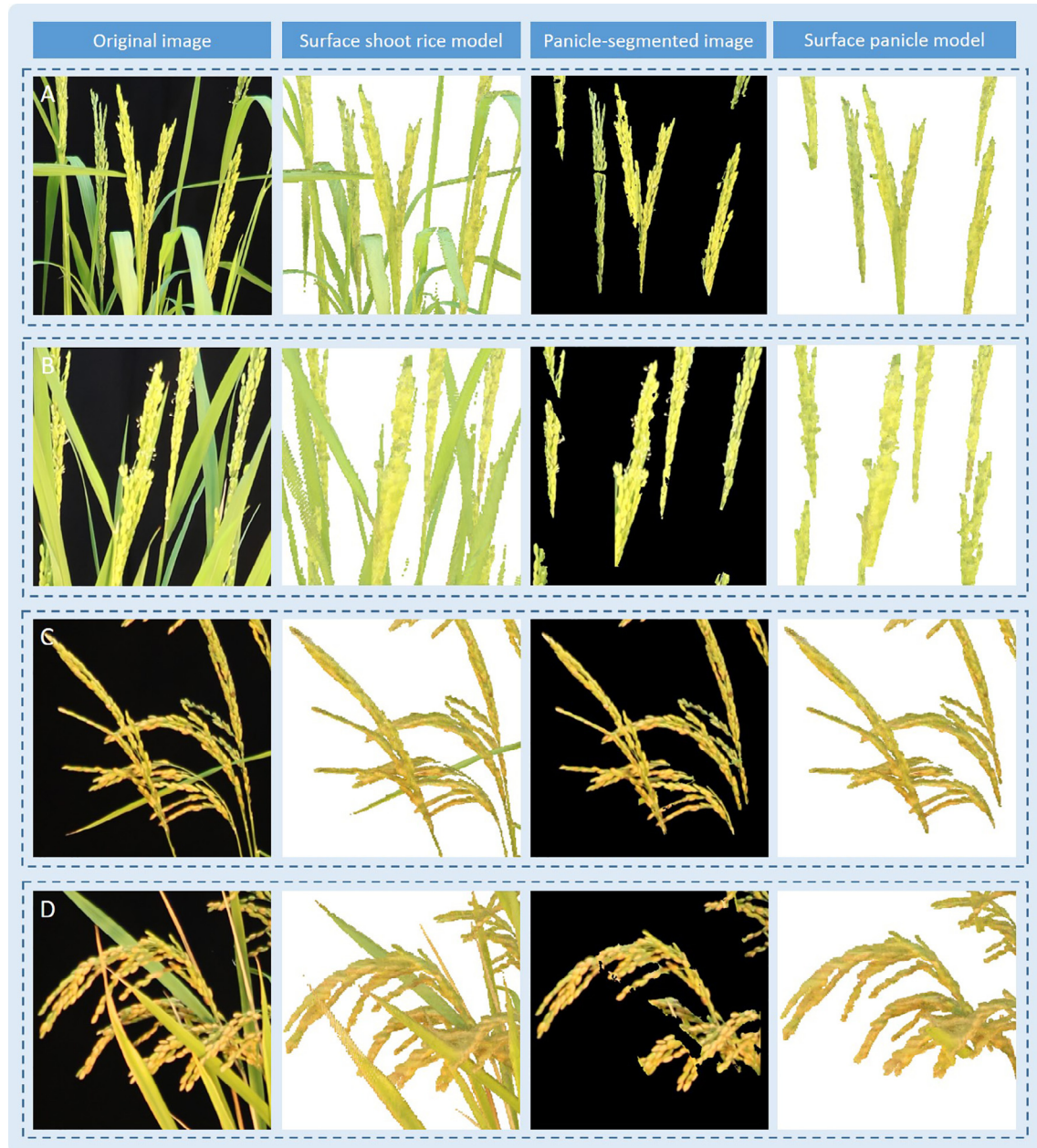


Fig. 6. The results of 3D shoot rice reconstruction and 3D panicle segmentation in local view at panicle level. The original rice images and the corresponding 2D panicle segmentation results are shown in the first and third columns, respectively. The surface shoot rice models and the surface panicle models are shown in the second and last columns. (A, B) Rice samples from 529 *O. sativa* accessions at the flowering stage. (C, D) Mutants of ZH11 at the mature stage.

Table 1
Efficiencies and accuracies of 3D panicle segmentation.

Item	Number of panicle-segmented images								
	3	5	6	9	10	15	30	45	90
Mean time cost (min)	0.83	0.94	1.04	1.15	1.16	1.40	2.14	2.82	5.10
SD of time cost	0.08	0.08	0.11	0.08	0.07	0.07	0.07	0.15	0.07
Mean accuracy (min)	0.86	0.88	0.89	0.91	0.92	0.93	0.94	0.94	0.95
SD of accuracy	0.06	0.06	0.06	0.05	0.05	0.04	0.04	0.03	0.03

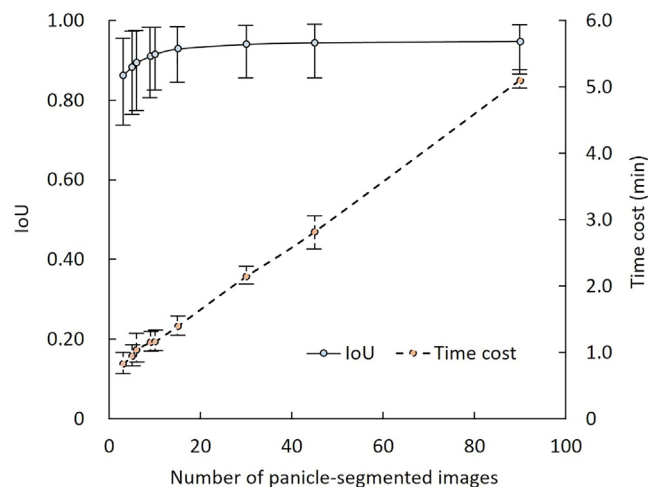


Fig. 7. The accuracies and efficiencies of 3D panicle segmentation using different numbers of panicle-segmented images.

the implementation of the codes have been provided in the supplementary files.

3. Results and discussion

3.1. Performance of 2D panicle segmentation

The comparison of the original rice images, ground-truth labels and segmentation results using the SegNet-Panicle model is shown in Fig. 4. The automatic segmentation results were highly consistent with the ground-truth labels. The precision, recall, IoU and F-measure of the 25 test images were respectively 0.84, 0.93, 0.79 and 0.88, also indicating that the SegNet-Panicle model could provide reliable 2D panicle segmentation results.

3.2. Performance of 3D shoot rice reconstruction and 3D panicle segmentation

The panicle modeling algorithm was tested on 50 rice plants. The results of four samples are shown in Fig. 5. For each sample,

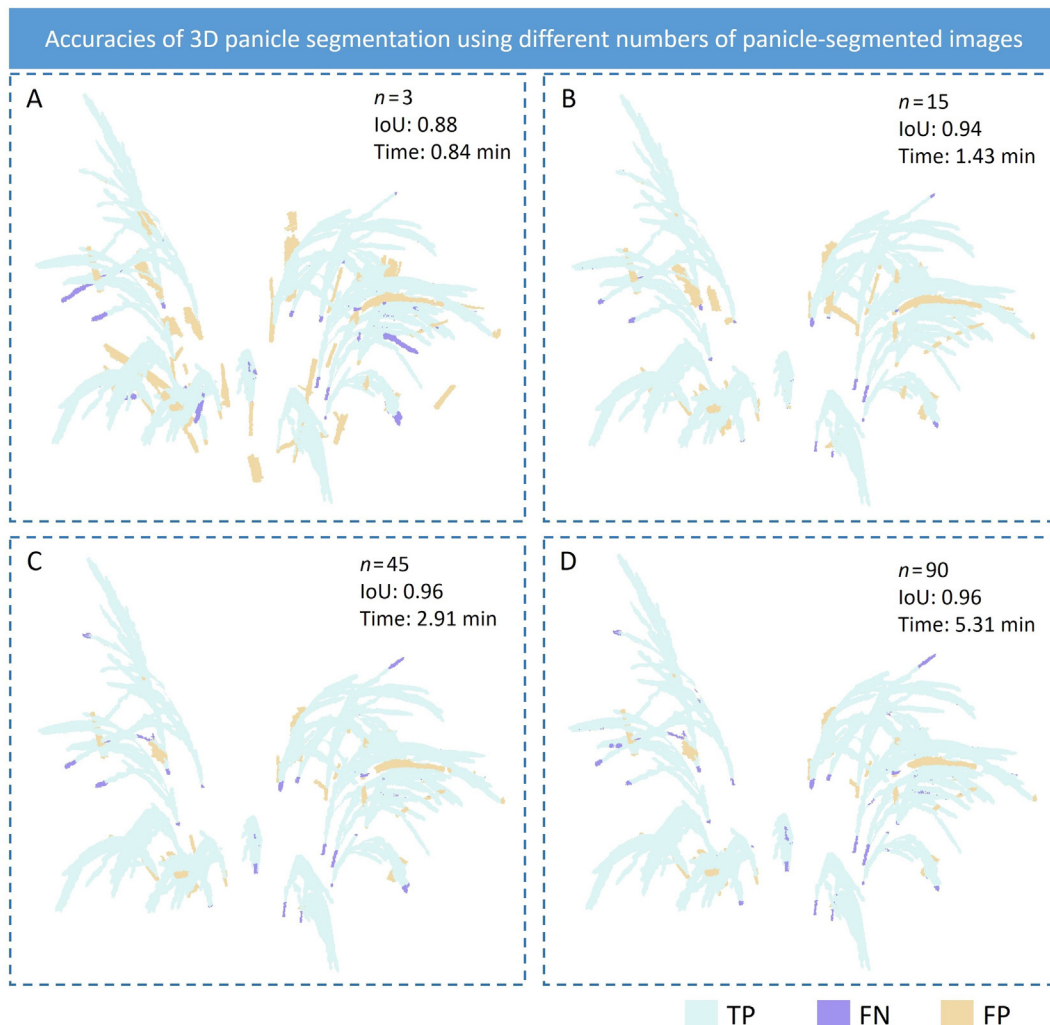


Fig. 8. The results of 3D panicle segmentation using different numbers of panicle-segmented images. n is the number of panicle-segmented images used in 3D panicle segmentation. TP, true positive; FN, false negative; FP, false positive.

one original rice image and the corresponding 2D panicle segmentation result are shown in the first column and the third column, respectively. The surface shoot rice model (SSRM) and the surface panicle model (SPM) of each sample were loaded using CloudCompare software. For comparison, the SSRM and SPM were rotated to an angle that was closest to the shooting angle of the selected original rice image, and the screenshots of the SSRM and the SPM from this view (side view) are displayed in the second and fourth columns, respectively. Screenshots of the SPMs from the top view are shown in the last column. For better observation, only panicle regions are shown in the third column. Comparing the third column with the fourth column, the SPMs were generally consistent with panicles in images, showing that the proposed algorithm was well qualified to recover the 3D shapes of rice panicles from multiview images. For sample A and B, images were taken at the flowering stage when panicles grew upright and appeared green. For sample C and D, images were taken at the mature stage, and

panicles were bent by the weight of the spikes and appeared yellow. The results showed that the algorithm was easily adaptable to rice plants of different accessions and growth stages. Besides, the reconstructed models are focused on panicle level and larger localized examples are provided in Fig. 6 for detailed comparison. The original rice images, the surface shoot rice models, the panicle-segmented images, and the surface panicle models are shown from the first to the last column, respectively. The texture of the reconstructed panicles could be easily observed. The videos of the reconstructed SRM, SSRM, PM, and SPM are represented in the supplementary files.

3.3. Processing efficiency

The training of SegNet and 2D panicle segmentation were conducted on the Ubuntu system. It took approximately 8.6 h to train the SegNet for 100 epochs through the training set. The execution



Fig. 9. Comparison of the reconstructed results of the proposed method with the SFM method. The surface shoot rice model and the surface panicle model by the SFM method are shown in the first and third columns, respectively, and the surface shoot rice model and the surface panicle model by the proposed method are shown in the second and last columns, respectively. The numbers are the point sizes of the models. (A) and (B) Rice samples from 529 *O. sativa* accessions at the flowering stage. (C) and (D) Mutants of ZH11 at the mature stage.

time for 2D panicle segmentation per rice sample using the SegNet-Panicle model was approximately 11.6 min. All the other processes were conducted on the Windows system. It took approximately 23.5 s to reconstruct the shoot rice model and 8.8 min to reconstruct the surface shoot rice model for a single rice plant when 90 images were used. The computational time for generating the panicle model and surface panicle model of a single rice plant varied from 0.8 to 5.1 min when different numbers of panicle-segmented images were used in the 3D panicle segmentation procedure. The whole process of panicle modeling for a rice plant was completed within 26 min.

3.4. Efficiency and accuracy of 3D panicle segmentation

The mean IoU and mean time cost when different numbers of panicle-segmented images were used in 3D panicle segmentation of 25 ZH11 mutants are shown in Fig. 7. The minimum and maximum values of the IoU and time cost are marked in the figure. The performance of 3D panicle segmentation was improved and the execution time increased when more panicle-segmented images were used. The mean IoU achieved the highest value of 0.95 when 90 panicle-segmented images were used. Detailed data of the efficiencies and accuracies are shown in Table 1. The segmentation

results obtained using 3, 15, 45, and 90 panicle-segmented images are shown in Fig. 8. TP, FN, and FP are marked in different colors. Smaller areas of FN and FP indicate higher accuracy. Although marked improvement is visible in the comparison of Fig. 8A with Fig. 8B, the results in Fig. 8B–D show little improvement. This finding is consistent with those shown in Fig. 7. Although the execution time increases proportionally, accuracy shows diminishing increases. Although there is a tradeoff between the accuracy and efficiency of 3D panicle segmentation, the execution time of this process can be reduced by half with almost no sacrifice of accuracy.

3.5. Comparison with structure from motion

The surface shoot rice models (SSRM-SFM) and the surface panicle models (SPM-SFM) based on VisualSfM are shown in respectively the first and third columns of Fig. 9. The surface shoot rice models (SSRM-SFS) and surface panicle models (SPM-SFS) generated by the proposed method are shown in respectively the second and last columns of Fig. 9. Comparing the last two columns, the surface panicle models generated by SFM method and the proposed method are similar overall. In detail, as shown in Fig. 10, with original rice images as references, many points are missing in SPM-SFM but were well recovered by SPM-SFS. This finding indi-

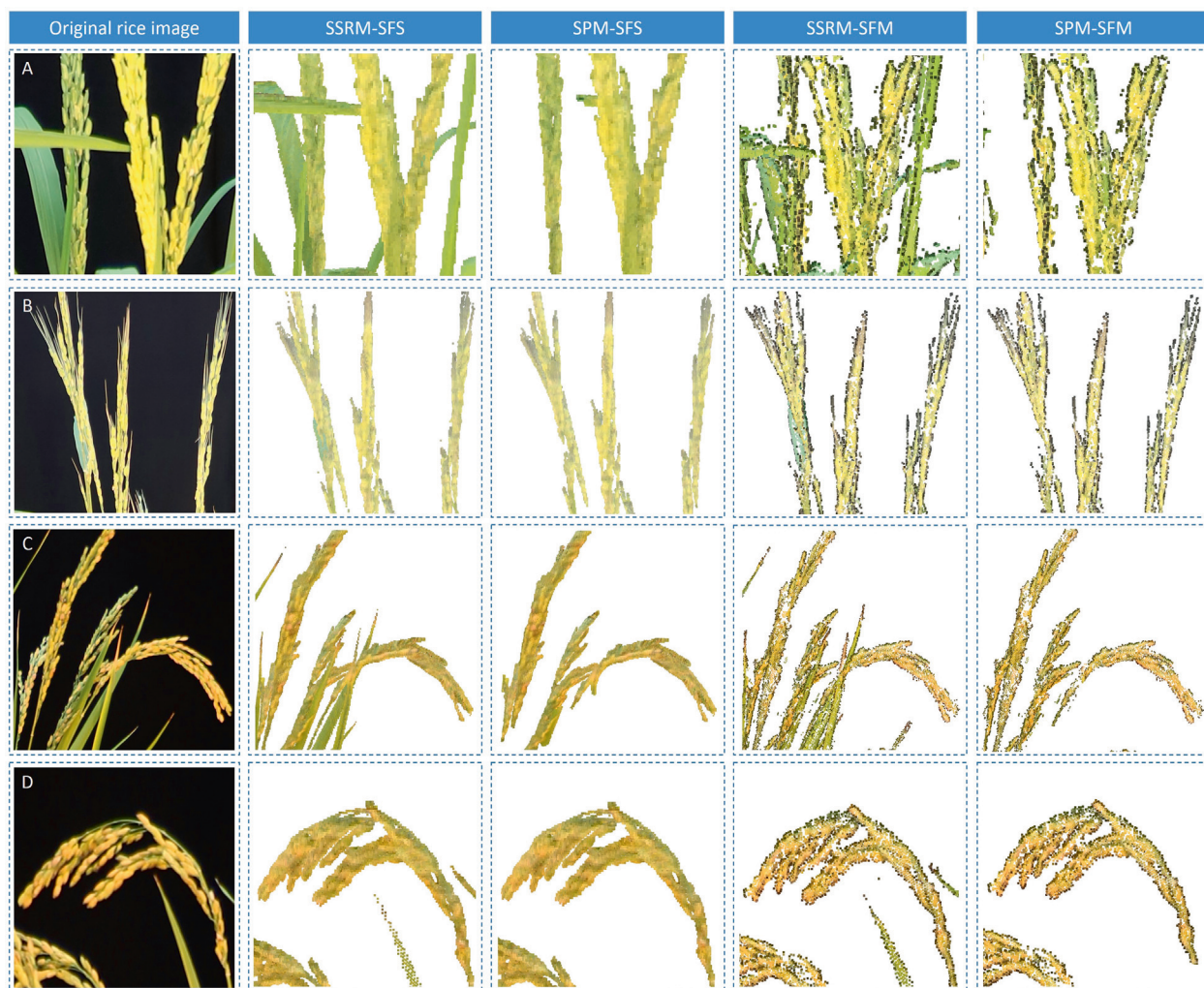


Fig. 10. Comparison of the reconstructed results of the proposed method with SFM method in local view at panicle level. The original rice images are shown in the first column. The surface shoot rice model and the surface panicle model by the proposed method are shown in the second and third columns, respectively. The surface shoot rice model and the surface panicle model by SFM method are shown in the fourth and the last column, respectively. (A) and (B) Rice samples from 529 *O. sativa* accessions at the flowering stage. (C) and (D) Mutants of ZH11 at the mature stage.

cates that the proposed method gave better performance with respect to shape and texture preservation in the case of rice panicles. From the aspect of efficiency, for a single rice plant, the processing time for the generation of the surface shoot rice model using 90 images by VisualSFM varied from 22 to 35 min. Tens more minutes were needed for manual segmentation on the SSRM-SFM by CloudCompare to obtain the final SPM-SFM. The execution time for all procedures of the proposed algorithm using 90 images for a single rice plant was no longer than 26 min. The proposed method was superior in processing efficiency as well.

3.6. Advantages and limitations

To our knowledge, automatic panicle segmentation of a 3D shoot rice model has not been described previously. In the proposed method, this issue was well addressed by using deep convolutional neural network and supervoxel clustering. The method is superior to a SFM-based method which needs subsequent manual processing in terms of texture preservation and computational efficiency.

The image acquisition is nondestructive, given that the panicle modeling algorithm requires multi-view images of the whole rice canopies instead of excised panicles. The developed low-cost (US \$ ~2000) multi-view imaging system is well adaptable for fully automatic high-throughput data acquisition if equipped with electromechanical controllers and automated conveyer.

The proposed algorithm was developed specially for indoor imaging systems, requiring a fixed camera and a pure rotation movement of the rice plant at constant speed. For this reason, it could not be applied in the field.

The validity is not guaranteed when the rice canopy is extremely dense. This limitation is common in visible image-based reconstructions and is unlikely to be eliminated unless other techniques such as computed tomography or magnetic resonance imaging are adopted. In addition, automatic acquisition of panicle traits such as panicle number, single-panicle length, and kernel number based on panicle models or surface panicle models remains a challenge, which should be relieved in the future work.

4. Conclusions

This paper described an automatic and nondestructive method for 3D modeling of rice panicles that combines shape from silhouette with a deep convolutional neural network and supervoxel clustering. The outputs of the algorithm for each rice plant are four 3D point clouds, including the shoot rice model, surface shoot rice model, panicle model, and surface panicle model. The image acquisition for a single rice plant was ~4 min and the image processing time was ~26 min when 90 images were used. The tradeoff between accuracy and efficiency involved in 3D panicle segmentation was assessed. Comparing the proposed algorithm with the widely used VisualSFM software, the proposed algorithm is superior with respect to texture preservation and processing efficiency. In future, we expect this method would be applied in high-throughput 3D phenotyping of large rice populations.

Data availability

Supplementary files for this article, which include source code, Panicle-3D technical documentation, evaluations of SFS reconstruction accuracy, and four videos of the reconstructed SRM, SSRM, PM, and SPM, can be retrieved from <http://plantphenomics.hzau.edu.cn/usercrop/Rice/download>.

Declaration of competing interest

The authors declare that they have no known competing financial interests or personal relationships that could have appeared to influence the work reported in this paper.

CRediT authorship contribution statement

Dan Wu: Data curation, Formal analysis, Methodology, Writing – original draft. **Lejun Yu:** Data curation, Formal analysis, Methodology, Writing – original draft. **Junli Ye:** Writing – review & editing. **Ruifang Zhai:** Software, Writing – review & editing. **Lingfeng Duan:** Software, Writing – review & editing. **Lingbo Liu:** Writing – review & editing. **Nai Wu:** Resources. **Zedong Geng:** Writing – review & editing. **Jingbo Fu:** Writing – review & editing. **Chenglong Huang:** Software, Writing – review & editing. **Shangbin Chen:** Software, Writing – review & editing. **Qian Liu:** Conceptualization, Funding acquisition, Project administration, Writing – review & editing. **Wanneng Yang:** Conceptualization, Funding acquisition, Project administration, Writing – review & editing.

Acknowledgments

This work was supported by the National Natural Science Foundation of China (U21A20205), Key Projects of Natural Science Foundation of Hubei Province (2021CFA059), Fundamental Research Funds for the Central Universities (2021ZKPY006), and cooperative funding between Huazhong Agricultural University and Shenzhen Institute of Agricultural Genomics (SZYJY2021005, SZYJY2021007).

References

- [1] T. Sasaki, B. Burr, International rice genome sequencing project: the effort to completely sequence the rice genome, *Curr. Opin. Plant Biol.* 3 (2000) 138–142.
- [2] T. Sasaki, The map-based sequence of the rice genome, *Nature* 436 (2005) 793–800.
- [3] J. Tu, G. Zhang, K. Datta, C. Xu, Y. He, Q. Zhang, G.S. Khush, S.K. Datta, Field performance of transgenic elite commercial hybrid rice expressing *Bacillus thuringiensis* δ-endotoxin, *Nat. Biotechnol.* 18 (2000) 1101–1104.
- [4] Q. Zhang, Strategies for developing green super rice, *Proc. Natl. Acad. Sci. U. S. A.* 104 (2007) 16402–16409.
- [5] S. Peng, G.S. Khush, P. Virk, Q. Tang, Y. Zou, Progress in ideotype breeding to increase rice yield potential, *Field Crops Res.* 108 (2008) 32–38.
- [6] X. Huang, Q. Qian, Z. Liu, H. Sun, S. He, D.A. Luo, G. Xia, C. Chu, J. Li, X. Fu, Natural variation at the DEP1 locus enhances grain yield in rice, *Nat. Genet.* 41 (2009) 494–497.
- [7] S. Sun, J. Yao, C. Wang, S. Yu, C. Xu, X. Li, Q. Zhang, Linking differential domain functions of the GS3 protein to natural variation of grain size in rice, *Proc. Natl. Acad. Sci. U. S. A.* 107 (2010) 19579–19584.
- [8] S. Donde, S. Mohapatra, B. Baksh, M. Padhy, S. Mukherjee, K. Roy, A. Chattopadhyay, P. Anandan, K. Swain, O. Sahoo, L. Singh, S. Dash Behera, Identification of QTLs for high grain yield and component traits in new plant types of rice, *PLoS ONE* 15 (2020) e0227785.
- [9] L. Li, Q. Zhang, D. Huang, A review of imaging techniques for plant phenotyping, *Sensors* 14 (2014) 20078–20111.
- [10] W. Yang, Z. Guo, C. Huang, L. Duan, G. Chen, N. Jiang, W. Fang, H. Feng, W. Xie, X. Lian, G. Wang, Q. Luo, Q. Zhang, Q. Liu, L. Xiong, Combining high-throughput phenotyping and genome-wide association studies to reveal natural genetic variation in rice, *Nat. Commun.* 5 (2014) 5087.
- [11] M.P. Pound, J.A. Atkinson, D.M. Wells, T.P. Pridmore, A.P. French, Deep learning for multi-task plant phenotyping, in: 2017 IEEE International Conference on Computer Vision Workshops (ICCVW), IEEE, Venice, Italy, 2017, pp. 2055–2063.
- [12] H. Lu, Z. Cao, Y. Xiao, B. Zhuang, C. Shen, TasselNet: counting maize tassels in the wild via local counts regression network, *Plant Methods* 13 (2017) 79.
- [13] X. Xiong, L. Duan, L. Liu, H. Tu, P. Yang, D. Wu, G. Chen, L. Xiong, W. Yang, Q. Liu, Panicle-SEG: a robust image segmentation method for rice panicles in the field based on deep learning and superpixel optimization, *Plant Methods* 13 (2017) 104.
- [14] L. Duan, C. Huang, G. Chen, L. Xiong, Q. Liu, W. Yang, Determination of rice panicle numbers during heading by multi-angle imaging, *Crop J.* 3 (2015) 211–219.
- [15] W. Wu, T. Liu, P. Zhou, T. Yang, C. Li, X. Zhong, C. Sun, S. Liu, W. Guo, Image analysis-based recognition and quantification of grain number per panicle in rice, *Plant Methods* 15 (2019) 122.

- [16] A.J. Burgess, R. Retkute, T. Herman, E.H. Murchie, Exploring relationships between canopy architecture, light distribution, and photosynthesis in contrasting rice genotypes using 3D canopy reconstruction, *Front. Plant Sci.* 8 (2017) 734.
- [17] S. Paulus, Measuring crops in 3D: using geometry for plant phenotyping, *Plant Methods* 15 (2019) 103.
- [18] Q. Guo, F. Wu, S. Pang, X. Zhao, L. Chen, J. Liu, B. Xue, G. Xu, L.E. Li, H. Jing, C. Chu, Crop 3D-a LiDAR based platform for 3D high-throughput crop phenotyping, *Sci. China Life Sci.* 61 (2018) 328–339.
- [19] Y. Su, F. Wu, Z. Ao, S. Jin, F. Qin, B. Liu, S. Pang, L. Liu, Q. Guo, Evaluating maize phenotype dynamics under drought stress using terrestrial lidar, *Plant Methods* 15 (2019) 11.
- [20] T.T. Nguyen, D.C. Slaughter, N. Max, J.N. Maloof, N. Sinha, Structured light-based 3D reconstruction system for plants, *Sensors* 15 (2015) 18587–18612.
- [21] S. Chaiwivatrakul, L. Tang, M.N. Dailey, A.D. Nakarmi, Automatic morphological trait characterization for corn plants via 3D holographic reconstruction, *Comput. Electron. Agric.* 109 (2014) 109–123.
- [22] J. Li, L. Tang, Developing a low-cost 3D plant morphological traits characterization system, *Comput. Electron. Agric.* 143 (2017) 1–13.
- [23] Y. Jiang, C. Li, A. Paterson, High throughput phenotyping of cotton plant height using depth images under field conditions, *Comput. Electron. Agric.* 130 (2016) 57–68.
- [24] M.P. Pound, A.P. French, E.H. Murchie, T.P. Pridmore, Automated recovery of three-dimensional models of plant shoots from multiple color images, *Plant Physiol.* 166 (2014) 1688–1698.
- [25] A.J. Burgess, R. Retkute, S.P. Preston, O.E. Jensen, M.P. Pound, T.P. Pridmore, E.H. Murchie, The 4-Dimensional plant: effects of wind-induced canopy movement on light fluctuations and photosynthesis, *Front. Plant Sci.* 7 (2016) 1392.
- [26] A. Burgess, R. Retkute, M. Pound, S. Mayes, E. Murchie, Image-based 3D canopy reconstruction to determine potential productivity in complex multi-species crop systems, *Ann. Bot.* 119 (2017) 517–532.
- [27] C. Wu, Towards linear-time incremental structure from motion, in: 2013 International Conference on 3D, Vision-3DV 2013., IEEE, Seattle, WA, USA, 2013, pp. 127–134.
- [28] Y. Furukawa, J. Ponce, Accurate, dense, and robust multiview stereopsis, *IEEE Trans. Pattern Anal. Mach. Intell.* 32 (2010) 1362–1376.
- [29] D. Zermas, V. Morellas, D. Mulla, N. Papanikopoulos, 3D model processing for high throughput phenotype extraction—the case of corn, *Comput. Electron. Agric.* 172 (2020) 105047.
- [30] J.Q. He, R.J. Harrison, B. Li, A novel 3D imaging system for strawberry phenotyping, *Plant Methods* 13 (2017) 93.
- [31] N. Briglia, K. Williams, D. Wu, Y. Li, S. Tao, F. Corke, G. Montanaro, A. Petrozza, D. Amato, F. Cellini, J. Doonan, W. Yang, V. Nuzzo, Image-based assessment of drought response in grapevines, *Front. Plant Sci.* 11 (2020) 595.
- [32] K.N. Kutulakos, S.M. Seitz, A theory of shape by space carving, *Int. J. Comput. Vis.* 38 (2000) 199–218.
- [33] S.M. Seitz, B. Curless, J. Diebel, D. Scharstein, R. Szeliski, A comparison and evaluation of multi-view stereo reconstruction algorithms, in: 2006 IEEE Computer Society Conference on Computer Vision and Pattern Recognition (CVPR'06), IEEE, New York, NY, USA, 2006, pp. 519–528.
- [34] J. Liang, A. Zia, J. Zhou, X. Sirault, 3D plant modelling via hyperspectral imaging, in: 2013 IEEE International Conference on Computer Vision Workshops, IEEE, Sydney, Australia, 2013, pp. 172–177.
- [35] J. Behmann, A.K. Mahlein, S. Paulus, H. Kuhlmann, E.C. Oerke, L. Plümer, Calibration of hyperspectral close-range pushbroom cameras for plant phenotyping, *ISPRS J. Photogramm. Remote Sens.* 106 (2015) 172–182.
- [36] J. Sandhu, F. Zhu, P. Paul, T. Gao, B. Dhatt, Y. Ge, P. Staswick, H. Yu, H. Walia, Pi-Plat: A high-resolution image-based 3D reconstruction method to estimate growth dynamics of rice inflorescence traits, *Methodology* 15 (2019) 162.
- [37] W. Hu, C. Zhang, Y. Jiang, C. Huang, Q. Liu, L. Xiong, W. Yang, F. Chen, Nondestructive 3D image analysis pipeline to extract rice grain traits using X-ray computed tomography, *Plant Phenomics* 2020 (2020) 1–12.
- [38] D. Maturana, S. Scherer, VoxNet: a 3D convolutional neural network for real-time object recognition, in: 2015 IEEE/RSJ International Conference on Intelligent Robots and Systems (IROS), IEEE, Hamburg, Germany, 2015, pp. 922–928.
- [39] R.Q. Charles, H. Su, M. Kaichun, L.J. Guibas, PointNet: deep learning on point sets for 3D classification and segmentation, in: 2017 IEEE Conference on Computer Vision and Pattern Recognition (CVPR), IEEE, Honolulu, HI, USA, 2017, pp. 77–85.
- [40] W. Xie, G. Wang, M. Yuan, W. Yao, K. Lyu, H. Zhao, M. Yang, P. Li, X. Zhang, J. Yuan, Q. Wang, F. Liu, H. Dong, L. Zhang, X. Li, X. Meng, W. Zhang, L. Xiong, Y. He, S. Wang, S. Yu, C. Xu, J. Luo, X. Li, J. Xiao, X. Lian, Q. Zhang, Breeding signatures of rice improvement revealed by a genomic variation map from a large germplasm collection, *Proc. Natl. Acad. Sci. U. S. A.* 112 (2015) E5411–E5419.
- [41] V. Badrinarayanan, A. Kendall, R. Cipolla, SegNet: a deep convolutional encoder-decoder architecture for image segmentation, *IEEE T. Pattern. Anal.* 39 (2017) 2481–2495.
- [42] Z. Zhang, A flexible new technique for camera calibration, *IEEE Trans. Pattern Anal. Mach. Intell.* 22 (2000) 1330–1334.
- [43] G. Bradski, The openCV library, *Dr. Dobbs J. Software Tools* 25 (2000) 120–126.
- [44] L. Bottou, Large-scale machine learning with stochastic gradient descent, in: Y. LeCun, G. Saporta (Eds.), *Proceedings of COMPSTAT*, Springer, Berlin, Germany, 2010.
- [45] C. Buehler, W. Matusik, L. Mcmillan, S. Gortler, Creating and rendering image-based visual hulls, *MIT LCS Technical Report* 780 (1999) 1–18.
- [46] J. Papon, A. Abramov, M. Schoeler, F. Wörgötter, Voxel cloud connectivity segmentation – supervoxels for point clouds, in: 2013 IEEE Conference on Computer Vision and Pattern Recognition, IEEE, Portland, OR, USA, 2013, pp. 2027–2034.
- [47] Adobe Inc., Adobe Photoshop, 2019, <https://www.adobe.com/products/photoshop.html>.
- [48] CloudCompare, <http://www.cloudcompare.org/main.html>.
- [49] R. Rusu, S. Cousins, 3D is here: Point cloud library (PCL), 2011, <https://doi.org/10.1109/ICRA.2011.5980567>.
- [50] R. Chandra, L. Dagum, D. Kohr, D. Maydan, J. McDonald, R. Menon, *Parallel Programming in OpenMP*, Morgan Kaufmann Publishers Inc., San Francisco, CA, USA, 2001.
- [51] NVIDIA, P. Vingelmann, F.H.P. Fitzek, CUDA, release: 10.2.89, 2020, <https://developer.nvidia.com/cuda-toolkit>.